

Kondo-Majorana coupling in Double Quantum Dots.

by

Jesús David Cifuentes Pardo

Advisor: Luis Gregorio Dias da Silva

MASTER OF SCIENCE

in

Instituto de Física

(Condensed Matter Physics)

UNIVERSIDADE DE SÃO PAULO

(R. do Matão, 1371 - Butantã, São Paulo)

February 11, 2019

© Jesús David Cifuentes Pardo 2017

Chapter 1

Abstract

In the last decades the interest in the “search of Majorana fermions” in condensed matter systems [1] has increased due to their potential applications in quantum computing. As recently as 2012, experimental works reporting the detection of such quasiparticles [2, 3]. Later works [4, 5, 6, 7], including a recent paper published by the advisor of this dissertation and collaborators [8], set out to explore the interplay of such Majorana zero-modes with strongly interacting systems such as semiconductor quantum dots, which can be readily integrated in the device. This research project aims to expand this idea using the numerical renormalization group to study the model of a double quantum dot coupled to metallic leads and to a topological superconductor supporting edge Majorana zero modes. This simple model allows the manipulation of the majorana modes bringing possible applications to braiding procedures . In addition, we will study the interplay of Kondo correlations, exchange interactions and Majorana physics.

Chapter 2

Table of Contents

1 Abstract	2
2 Table of Contents	3
3 Coupling the Majorana Zero Mode to a Double Quantum Dot	4
3.1 Non-interacting case	5
3.1.1 The Green function:	5
3.1.2 MZM manipulation	7
3.2 Interacting Results	11
3.2.1 a) Removing Kondo and Majorana with QD-interference	15
3.2.2 b) Indirect Majorana after Removing Kondo with QD-interference	17
3.2.3 e) Transferring the MZM through gate voltage shifting ε_2 .	20
3.3 Particle-Hole symmetric shifting of $\varepsilon_2 = \frac{U}{2}$.	24
3.4 Shifting t_2	24
References	26
Bibliography	26

Appendices

A Appendix	28
A.1 From the logarithmic discretization to the Wilson's chain.	28
B Three peak appearance in the Double Quantum Dot model.	33
B.1 Initial DQD-Majorana Hamiltonian.	34

Chapter 3

Coupling the Majorana Zero Mode to a Double Quantum Dot

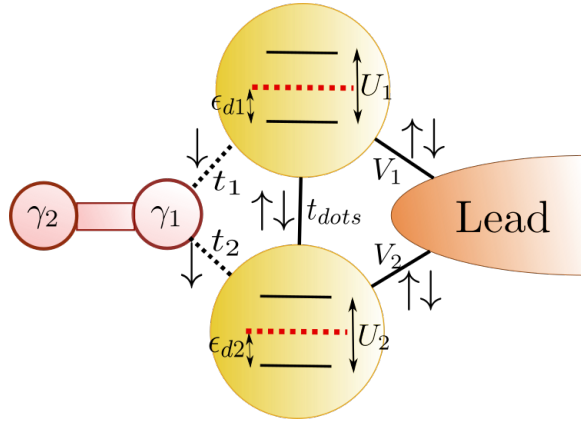


Figure 3.1: General model. [Source: [By the Author](#)

The idea of using Majorana islands formed by QDs coupled to topological superconducting wires has recently turned on new lights into the fabrication of of quantum architectures [9, 10]. The main insight of this method is that todayâs precise experimental control over the parameters of QDs -energy levels, tunneling couplings, etc.- offers the unique possibility of manipulating the Majorana modes inside multi-dot systems. The simplest case where Majorana manipulation is possible is in a double quantum dot. So far, no complete analysis of this basis case has been done. The purpose of this chapter is to fill this gap by realizing a full quantum transport study of the effects of coupling a Majorana mode with a double quantum dot. For this, we combine the ballistic transport and the NRG approach developed in ??.

We consider the model in Figure 3.1 which can be obtained from the combination of Hamiltonians of a QD-Majorana (??) and a DQD (??). The Hamiltonian

$$H = \sum_{i=1}^2 \sum_{k,\sigma} \left(\varepsilon_i + \frac{U_i}{2} \right) d_{i\sigma}^\dagger d_{i\sigma} + \frac{U_i}{2} (d_{i\sigma}^\dagger d_{i\sigma} - 1)^2 + t_i (\gamma d_{i,\downarrow} + d_{i,\downarrow}^\dagger \gamma) + V_i d_{i\sigma}^\dagger c_{k\sigma} + V_i^* c_{k\sigma}^\dagger d_{i\sigma}. \quad (3.1)$$

3.1 Non-interacting case

In order to understand the physical properties of this model, we probed a set of thought processes. The main variable in this analysis is the density of states. We will observe its evolution on both QDs under the tuning of the model parameters such as the majorana couplings (t_1, t_2) , gate voltages ($\varepsilon_1, \varepsilon_2$) and the inter dot coupling (t_{dots}). With these processes intend to show whether it is possible to "manipulate" the majorana modes inside the dots by tuning the established parameters. The number of possible combinations of parameters is huge and not all of them lead to important results. So on, we used the ballistic transport to select which arrangements could bring novel results. The most interesting models were simulated with NRG in the interacting case ??.

3.1.1 The Green function:

This new model is a combination the DQD graph (??) with the Majorana-QD graph ??b). We can use the trick in ?? to get rid of the of the Green function $G_{f_\downarrow, d_1^\dagger}(\omega)$ for the second Majorana operator. This allows us to obtain the following transport equations

$$\begin{bmatrix} \omega - \varepsilon_1 & -V_1^* & -t_{dots} & -T_1 & 0 & 0 & 0 \\ -V_1 & \omega - \varepsilon_k & -V_2 & 0 & 0 & 0 & 0 \\ -t_{dots}^* & -V_2^* & \omega - \varepsilon_2 & -T_2 & 0 & 0 & 0 \\ -T_1^* & 0 & -T_2^* & \omega - \varepsilon_M & -T_2^* & 0 & -T_1 \\ 0 & 0 & 0 & -T_2 & \omega + \varepsilon_2 & V_2^* & t_{dots}^* \\ 0 & 0 & 0 & 0 & V_2 & \omega + \varepsilon_k & V_1 \\ 0 & 0 & 0 & -T_1 & t_{dots} & V_1^* & \omega + \varepsilon_1 \end{bmatrix} \begin{bmatrix} G_{d_{1\downarrow}, d_{1\downarrow}^\dagger}(\omega) \\ G_{c_{k\downarrow}, d_{1\downarrow}^\dagger}(\omega) \\ G_{d_{2\downarrow}, d_{1\downarrow}^\dagger}(\omega) \\ G_{f_\downarrow, d_{1\downarrow}^\dagger}(\omega) \\ G_{d_{2\downarrow}^\dagger, d_{1\downarrow}^\dagger}(\omega) \\ G_{c_{k\downarrow}^\dagger, d_{1\downarrow}^\dagger}(\omega) \\ G_{d_{1\downarrow}^\dagger, d_{1\downarrow}^\dagger}(\omega) \end{bmatrix} = \begin{bmatrix} 0 \\ 0 \\ 0 \\ 0 \\ 0 \\ 0 \\ 1 \end{bmatrix}, \quad (3.2)$$

where $T_i = \frac{t_i}{\sqrt{\omega + \varepsilon_M}}$.

The graph representing this equation is Figure 3.2.a). Using the algorithm in ?? we start to popping the vertexes $c_k, c_k^\dagger, d_{2,\downarrow}$ and $d_{2,\downarrow}^\dagger$ in that order. The energies associated to $d_{1,\downarrow}$ and $d_{1,\downarrow}^\dagger$ will be similar to the energy of the DQD (??) giving

$$\varepsilon_{DQD}^\pm = \pm \varepsilon_1 + \sum_{\mathbf{k}} \frac{V_1 V_1^*}{\omega - \varepsilon_{\mathbf{k}}} + \frac{\left\| \pm t_{dots} + \sum_{\mathbf{k}} \frac{V_1 V_2^*}{\omega - \varepsilon_{\mathbf{k}}} \right\|^2}{\omega \pm \varepsilon_2 - \sum_{\mathbf{k}} \frac{V_2 V_2^*}{\omega - \varepsilon_{\mathbf{k}}}}. \quad (3.3)$$

There is also a correction in the couplings between the Majorana mode and $d_{1,\downarrow}, d_{1,\downarrow}^\dagger$ given by

$$T_\pm = \pm t_1 \pm t_2 \frac{\left(\pm t_{dots} + \sum_{\mathbf{k}} \frac{V_1 V_2^*}{\omega - \varepsilon_{\mathbf{k}}} \right)}{\omega \pm \varepsilon_2 \pm \sum_{\mathbf{k}} \frac{V_2 V_2^*}{\omega - \varepsilon_{\mathbf{k}}}}. \quad (3.4)$$

3.1. Non-interacting case

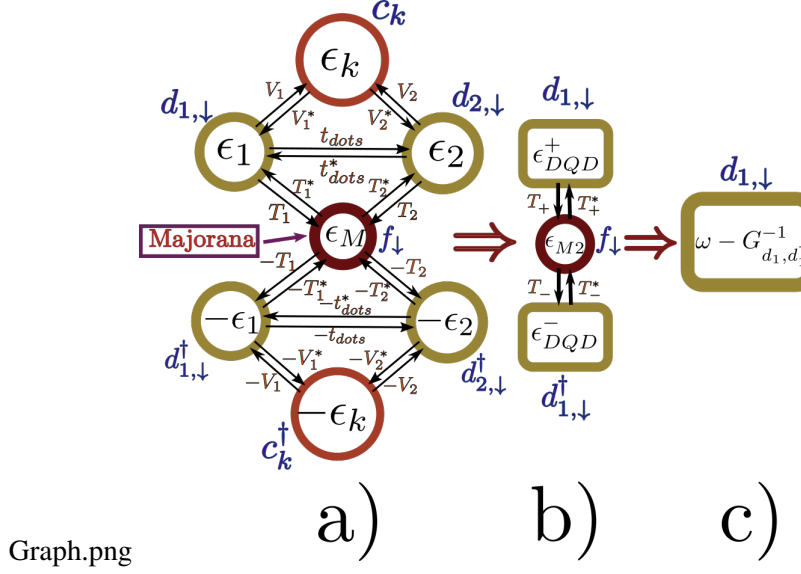


Figure 3.2: Graph method applied to a DQD coupled to a Majorana zero mode. a) Initial stage. b) Popped vertexes c_k^\dagger , c_k , $d_{2,\downarrow}$, $d_{2,\uparrow}$ in that order. c) Popped vertexes $d_{1,\uparrow}^\dagger$ and f_\downarrow , the final energy is $\omega - G_{d_{1,\downarrow}^\dagger}^{-1}(\omega)$.

Source: By the Author

In addition since the Majorana is in contact with dot 2, there is an extra-term appearing in the Majorana energy given by

$$\epsilon_{M2} = \omega - \epsilon_M - \frac{\frac{\omega}{\omega + \epsilon_M} \|t_2\|^2}{\omega - \epsilon_2 - \sum_k \frac{V_2 V_2^*}{\omega - \epsilon_k}} - \frac{\frac{\omega}{\omega + \epsilon_M} \|t_2\|^2}{\omega + \epsilon_2 - \sum_k \frac{V_2 V_2^*}{\omega + \epsilon_k}}. \quad (3.5)$$

It only remains to pop out vertexes $d_{1,\uparrow}^\dagger$ and f_\downarrow in that order to obtain the green function

$$G_{d_{1,\downarrow}, d_{1,\uparrow}^\dagger}(\omega) = \frac{1}{\omega - \epsilon_{DQD}^+ - \frac{\|T_+\|^2}{\omega - \epsilon_{M2} - \frac{\|T_-\|^2}{\epsilon_{DQD}}}}. \quad (3.6)$$

This simple formula summarizes the transport information through the first dot of the non-interacting Majorana-DQD system. To compute the DOS we just need to replace once again $\sum_k \frac{V_1 V_1^*}{\omega - \epsilon_k} = -i\Gamma_1$ as performed in ???. By plotting the final DOS in Mathematica we were able to observe the transitions of the Majorana mode while manipulating the model parameters.

3.1. Non-interacting case

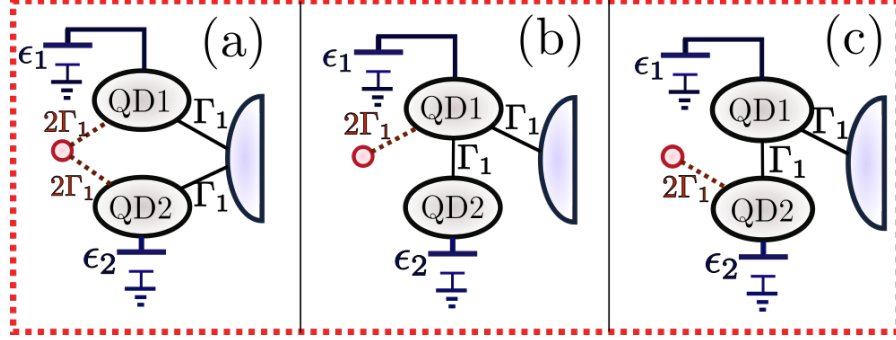


Figure 3.3: . Source: *By the Author*

3.1.2 MZM manipulation

The density of states provides significant information about the presence of a Majorana zero modes in the dot. We characterize the Majorana signature by a robust zero-mode with two possible heights:

- **Type I:** The spin- \downarrow DOS is the half of the spin- \uparrow DOS at the Fermi energy ($\rho_{\downarrow}(0) = \rho_{\uparrow}(0)$).
- **Type II:** A spin- \downarrow zero mode of height $\rho_{\downarrow}(0) = \frac{0.5}{\pi\Gamma_1}$.

In our results we observe several times these two types of signatures. Type I often appears when there is a zero-mode in the spin- \uparrow DOS. Type II emerges in the remaining situations.

We call MZM manipulation to the "movements" attributed to the Majorana signature under the tunning of the dot gate voltages ($\varepsilon_1, \varepsilon_2$). This manipulation process is performed in three different set ups that are presented in Fig. Figure 3.3 with definite values of Γ_2 , t_{dots} , t_1 and t_2 . In configuration (a), we coupled the QD symmetrically to the lead and the Majorana mode. With this setup we expect to break the localization of the MZM which should split and tunnel into both dots. In setups (b) and (c) we coupled the second dot indirectly through the first dot. Hence, quantum interference should split the zero mode in two states. Our objective is to observe what occurs with the Majorana signature in this situation. There are two options to connect the MZM in this situation. Attached it directly through the first dot (b) or indirectly through the second dot (c).

3.1. Non-interacting case

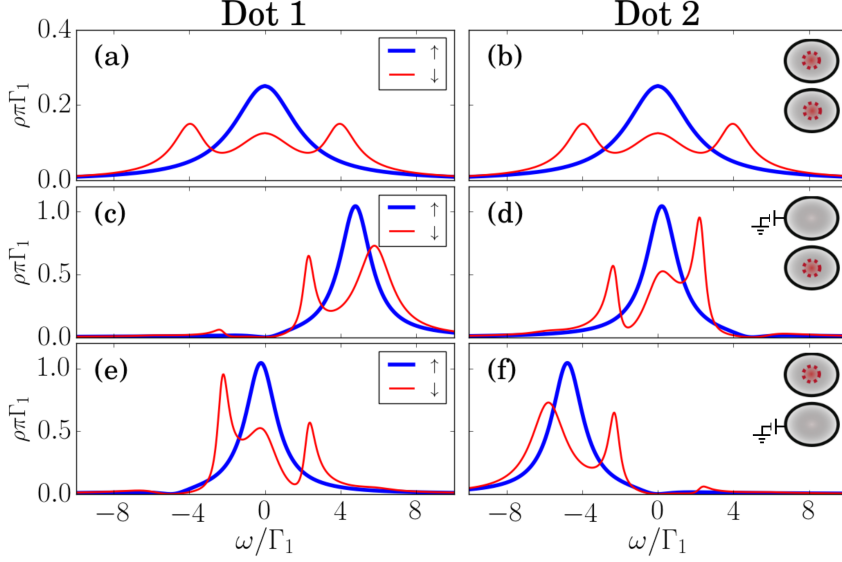


Figure 3.4: Non-interacting DOS in the symmetric coupling setup (Fig. Figure 3.3(a)) at each QD. First column: Dot 1. Second column: Dot 2. The gate voltages vary at each row. First row: Zero gate voltages $\varepsilon_1 = \varepsilon_2 = 0$. Second row: $\varepsilon_1 = 5\Gamma_1$, $\varepsilon_2 = 0$. Third row: $\varepsilon_1 = 0$, $\varepsilon_2 = -5\Gamma_1$. Bold blue lines: Spin- \uparrow DOS. Thin red lines: Spin- \downarrow DOS. The insets at the right show which dot carries a Majorana signature, represented by a red dashed circle. Upper: First dot. Lower: Second dot.

The non-interacting results for setups (a),(b) and (c) of FIG.Figure 3.3 are shown at figures FIG.Figure 3.4, FIG.Figure 3.5 and FIG.Figure 3.16 respectively. Each figure depicts the DOS of dot 1(left) and dot 2(right). The gate voltage is initially 0 in both dots at the first row. In the second row the gate voltage is turned on to $\varepsilon_1 = 5\Gamma_1$ in the first dot and remains at $\varepsilon_2 = 0$ in the second dot. In the third row the first dot's voltage is off $\varepsilon_1 = 0$ and we switch on the second dot with a negative voltage of $\varepsilon_2 = -5\Gamma_1$. The insets at each row shows which dots exhibit Majorana signatures, depicted by a red dashed circle inside the dot. These images will continuously change under the tuning of gate voltages which represents the manipulation of the Majorana signature.

In FIG.Figure 3.4 we observe the results for the symmetric coupling setup FIG.Figure 3.3(a). In the particle hole symmetric case (first row) the DOS is equal in both dots. Note that that the spin- \downarrow (Thin red line) DOS is the half of the spin- \uparrow (Bold blue line) DOS at the Fermi energy ($\rho_{\downarrow}(0) = \frac{1}{2}\rho_{\uparrow}(0)$). This type II Majorana signature is similar to the one observed when a single dot is coupled to a Majorana mode. [4] We may conclude that the Majorana in tunneling inside both dots breaking the localization of the MZM. If a positive or negative gate voltage is induced in one of the dots, as shown in the second and third row of Figure Figure 3.4(c)-(f), the

3.1. Non-interacting case

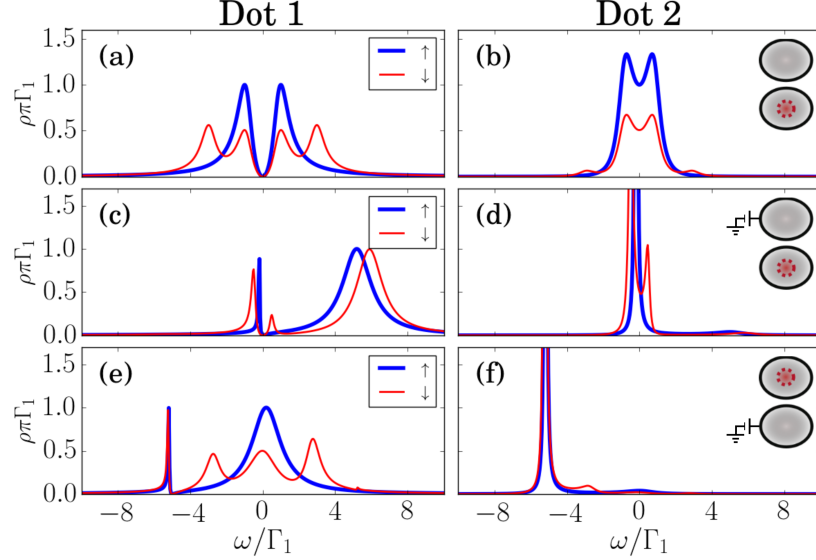


Figure 3.5: Non-interacting DOS of the setup in Fig. Figure 3.3(b). (b). First line (a),(b): $\epsilon_1 = \epsilon_2 = 0$. Second line (c),(d): $\epsilon_1 = 5\Gamma_1$, $\epsilon_2 = 0$. Third line (e),(f): $\epsilon_2 = -5\Gamma_1$, $\epsilon_1 = 0$. Blue bold lines: Spin- \uparrow DOS. Red thin lines: Spin- \downarrow DOS. The inset at the upper-right corner of each line indicates which dots exhibit Majorana signature, which is represented by a red dashed circle inside the dot.

Majorana zero mode vanishes from that dot. Meanwhile the density of states in the other dot increases while preserving the Majorana signature. This means that the MZM is actually being induced to "leave" this dots and leak into the other dot by the gate voltage activation. This first example of MZM manipulation.

Another example of MZM manipulation occurs when the second dot is not directly connected to the lead. In this case, the inter-dot tunneling generates quantum interference which finally destroys the central peak as observe in FIG. Figure 3.5(a) at the spin- \uparrow DOS . The spin- \downarrow channel at FIG. Figure 3.5(a), which is coupled to the MZM, does not exhibit the characteristic Fermi peak either. Instead, the one half Majorana signature at the Fermi energy ($\rho_{\downarrow}(0) = \frac{1}{2}\rho_{\uparrow}(0)$) appears clearly inside the second dot FIG. Figure 3.5(b). This situation prevails when the first dot's gate voltage is turned on FIG. Figure 3.5(c)&(d). While the first dot does not seem to exhibit any type of Majorana signature, the second dot's spin- \downarrow DOS exhibits a robust zero-mode of height $\frac{0.5}{\pi\Gamma}$. The results are more exciting when the second dot's gate voltage is turned on in FIG. Figure 3.5(e)&(f). These figures clearly show how the MZM, previously localized at the second dot, is induced to leave this dot and returned onto the first dot. Moreover, the DOS of spin- \uparrow and spin- \downarrow channels are very similar to the spectral densities observed at FIG. Figure 3.4(d)(e), which means that the previous interference pattern has disappeared due

3.1. Non-interacting case

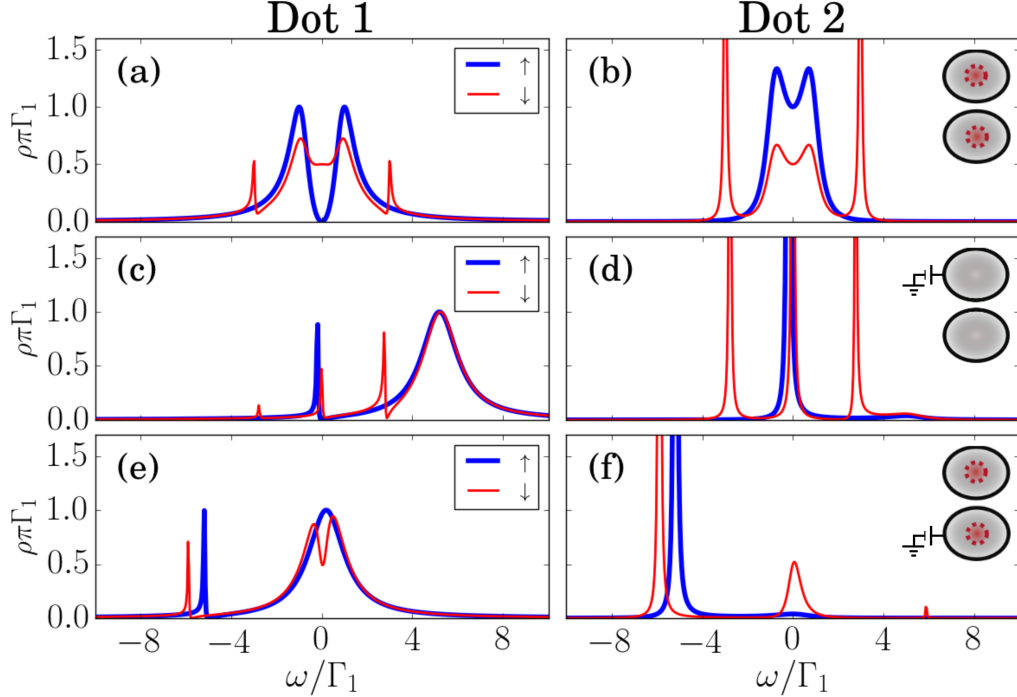


Figure 3.6: Non-interacting DOS of the set up in Fig. Figure 3.3(c). First line (a),(b): $\epsilon_1 = \epsilon_2 = 0$. Second line (c),(d): $\epsilon_1 = 5\Gamma_1$, $\epsilon_2 = 0$. Third line (e),(f): $\epsilon_2 = -5\Gamma_1$, $\epsilon_1 = 0$. Blue bold lines: Spin- \uparrow DOS. Red thin lines: Spin- \downarrow DOS. The inset at the upper-right corner of each line indicates which dots exhibit Majorana signature, which is represented by a red dashed circle inside the dot.

to the presence of this gate voltage.

The results of the third configuration FIG. Figure 3.3(c) appear in FIG. Figure 3.16. Contrary to what was observed in the previous case, this time the Majorana signature is not destroyed by the interference but instead, the $\frac{0.5}{\pi\Gamma}$ -height MZM emerges indirectly in the first dot. This is a perfect way to separate the Majorana's spin- \downarrow DOS from the central spin- \uparrow zero-mode which is still destroyed by the interference. In addition, the second dot still exhibits a type I Majorana signature as observed in FIG. Figure 3.16(b). In the second row we observe that turning on the gate voltage in dot 1 destroys the Majorana signature in both dots FIG. Figure 3.16(c)(d). On the other hand, if the second dot's voltage is switched both dots will preserve their Majorana signature (QD1:type I, QD2: type II), while the spin- \uparrow quantum interference vanishes in the first dot.

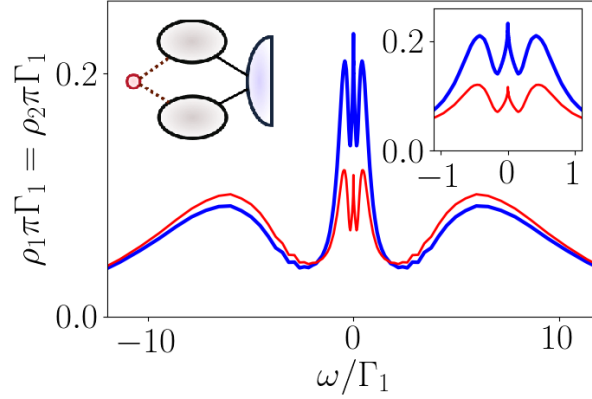


Figure 3.7: Density of states of both dots in the symmetric coupling without gate voltages between the Majorana and the interacting DQD. Bold blue lines: Spin- \uparrow DOS. Thin red lines: Spin- \downarrow DOS. Inset: Low-energy DOS.

3.2 Interacting Results

Now we consider a Coulomb repulsion energy of $U = 17\Gamma_1$ in both dots. The factor $\frac{U_i}{2}(\sum_{\sigma}\hat{n}_{i\sigma} - 1)^2$ in (??) favors states with an odd number of electrons (and holes). In addition, particle-hole equilibrium is now achieved when $(\epsilon_{di} + \frac{U_i}{2})\hat{n}_{i\sigma}$. Any induced gate voltage must be considered as a shifting from this equilibrium point. FIGFigure 3.7 shows the DOS at both QDs for the symmetric coupling configuration Figure 3.3. The two peaks appearing at around $8.6\Gamma_1 = \frac{U_i}{2}$ represent the two energy levels spaced by the Coulomb repulsion factor U . The central spin- \uparrow peak is a consequence of the Kondo effect, [11, 12] while the two satellite peaks observed in the inset are the result of the RKKY indirect interaction between both dots. [13, 14, 15] Moreover, the system presents a Majorana signature characterized by half spin- \downarrow DOS at the Fermi energy ($\rho_{\downarrow}(0) = \frac{1}{2}\rho_{\uparrow}(0)$). Note, that in this case the Majorana signature coexists with the Kondo effect in the DQD as already predicted by Ruiz-Tijerina *et al.* for a single dot. [8]

In this part project we are interested in the physics at low energy scales $\omega \sim \Gamma_1$ close to the Kondo and MZM temperature. At this scale we can observe similar results with the non-interacting results. For instance, FIG.Figure 3.8 shows the NRG results for the symmetric setup in FIG.Figure 3.3(a). In agreement with the non-interacting results, both dots have type I Majorana signatures. These signatures can be manipulated by tuning one of the dot's gate voltage to induce the MZM to leak into the other dot. The DOS at figures FIG.Figure 3.8(d)(e) shows a type I Majorana signature with $\rho_{\downarrow}(0) \approx \frac{1}{2}\rho_{\uparrow}(0)$. We observed that this Majorana signature is stable for adjustments of energies below the $6\Gamma_1$. At larger gate voltages the signal is destroyed.

In the second setup FIG.Figure 3.3(b), the NRG results in FIG.Figure 3.12 exhibit Majo-

3.2. Interacting Results

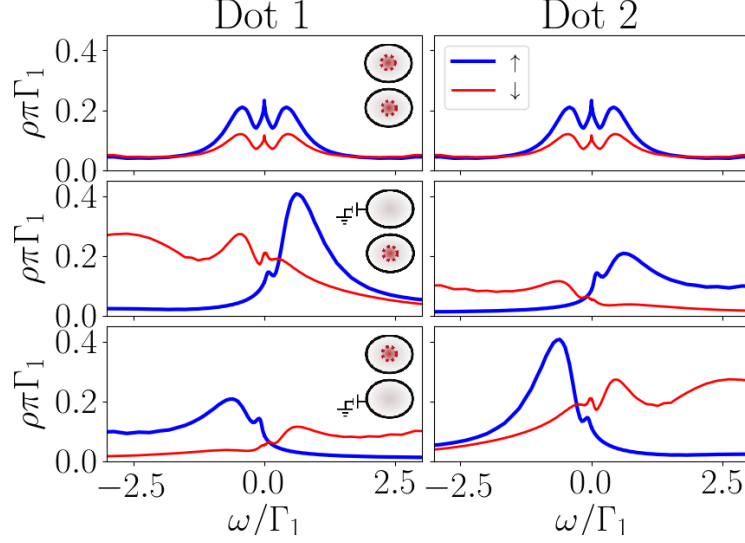


Figure 3.8: The same as in FIG. Figure 3.4 for the interacting DOS in the symmetric coupling setup (Fig. Figure 3.3).

Majorana signatures similar to the non-interacting case. In the first row, the Majorana signature is destroyed by quantum interference while the second dot presents a type I Majorana signature as can be observed in the inset of the second dot. The first difference occurs when the gate voltage is switched on the first dot. This time the Majorana mode jumps onto the first dot which presents a type I Majorana signature . If the voltage is switched on the second dot, a type 2 Majorana signature appears at very low energies in dot 1.

3.2. Interacting Results

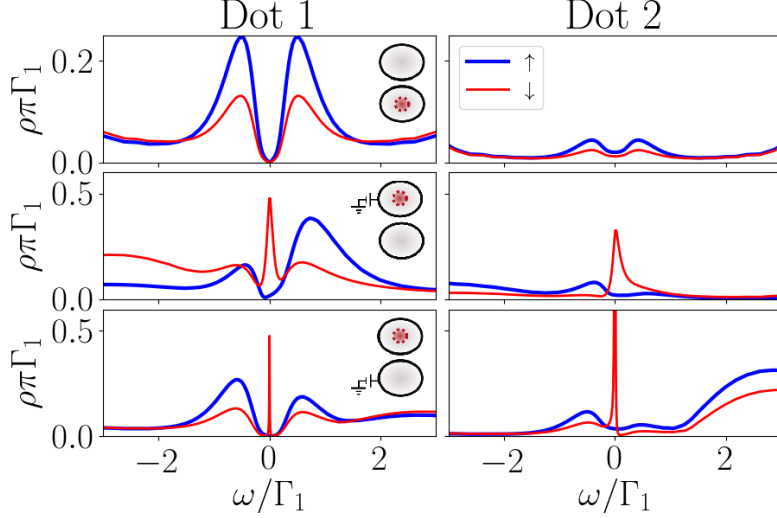


Figure 3.9: The same as in FIG. Figure 3.4 for the interacting DOS of the setup in Fig. Figure 3.3(b). Inset in b): Low-energy DOS.

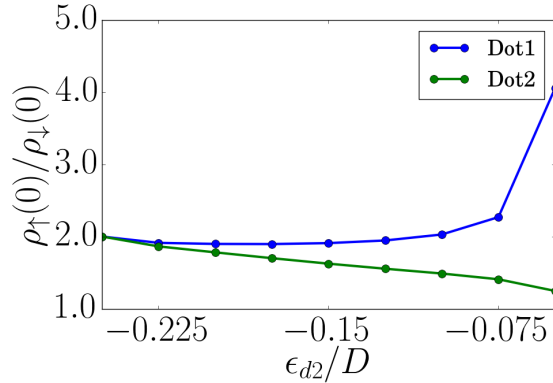


Figure 3.11: As described in section 3.2.2 the relation $\frac{\rho_1(0)}{\rho_2(0)} = 2$ constitutes a Majorana Signature . This picture evaluates shows the evolution of the relation $\frac{\rho_1(0)}{\rho_2(0)}$ for both QDs. While QD2 losses rapidly the Majorana signature, QD1 maintains it till $\varepsilon_2 \sim -0.1$.

Finally, FIG.?? show the NRG results for the last configuration FIG. Figure 3.3(c). Surprisingly, the indirectly attached MZM exhibits a robust type II Majorana signature in the first dot over a destroyed Kondo peak. This signature is stable under the gate voltage tuning. In addition, only the first in the particle hole symmetric case the second dot presents a type II Majorana signature (Inset FIG.??(b)). The difference between this model and the other that leads to a stable

3.2. Interacting Results

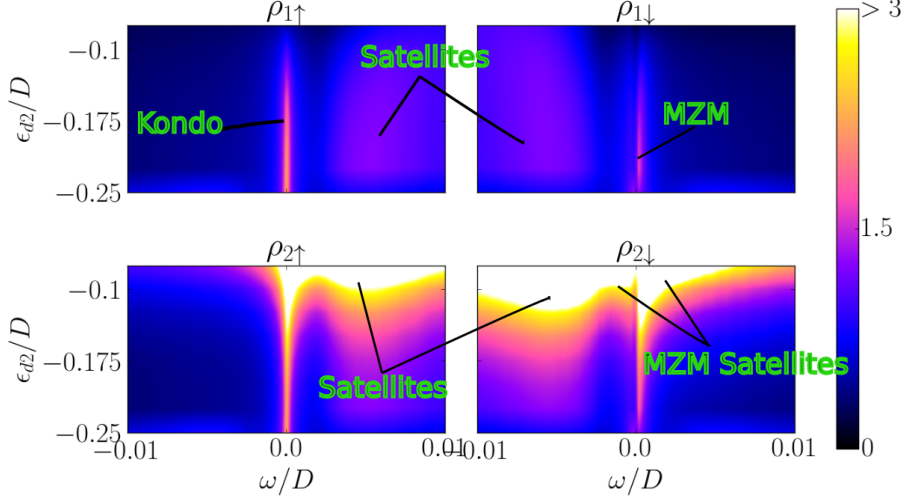


Figure 3.10: Evolution of the DOS of both QDs through the ϵ_2 tuning. UP: QD1. DOWN: QD2. LEFT: Spin \uparrow . RIGHT: Spin \downarrow .

signature in one of the dots occurs because the QD's in the (c) model are connected in series. Therefore, the Majorana mode will always prevail in the dot that is attached to the leads besides the application of gate voltages. This case is similar to the model of a single dot attached to a Majorana chain, where it is known that the Majorana signatures is not disturbed by the gate tuning.

3.2. Interacting Results

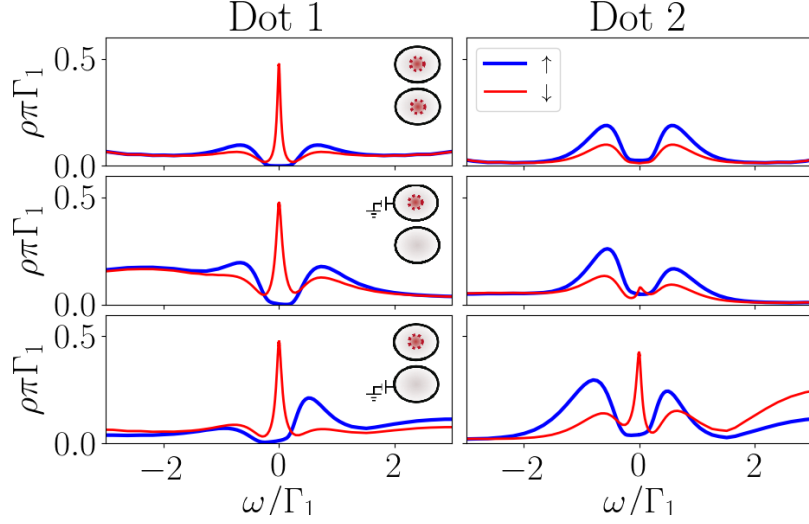


Figure 3.12: The same as in FIG. Figure 3.4 for the interacting DOS of the setup in Fig. Figure 3.3(b). Inset in b): Low-energy DOS.

3.2.1 a) Removing Kondo and Majorana with QD-interference

Note *Text coming soon*

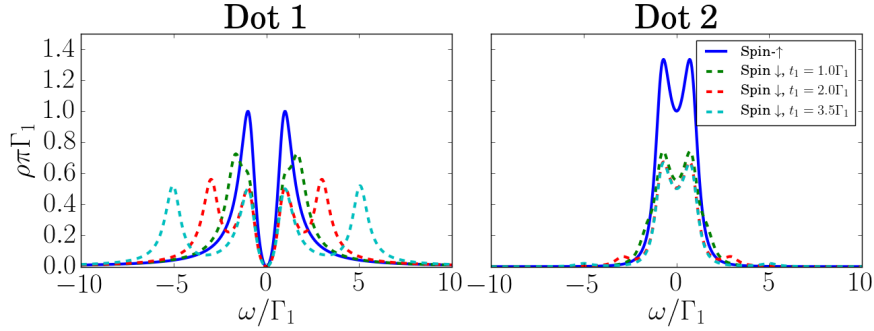


Figure 3.19: Source: By the Author

3.2. Interacting Results

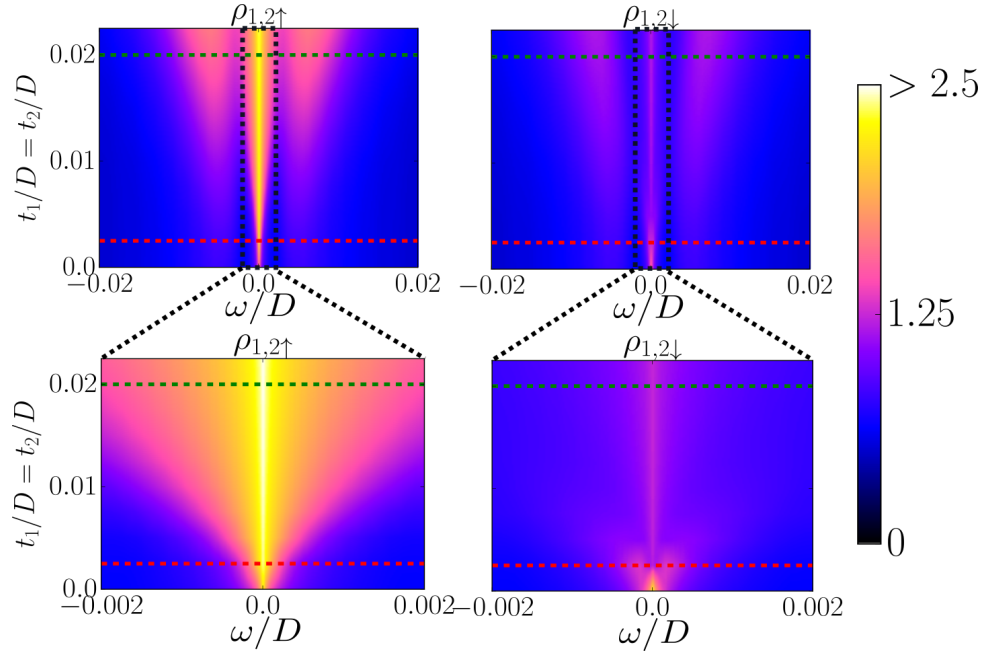


Figure 3.13: Evolution of the DOS of both QDs through $t_1 = t_2$ tuning. UP: Energy scale $\omega \sim 10^{-2}D$. DOWN: Energy scale $\omega \sim 10^{-3}D$. LEFT: Spin \uparrow . RIGHT: Spin \downarrow .

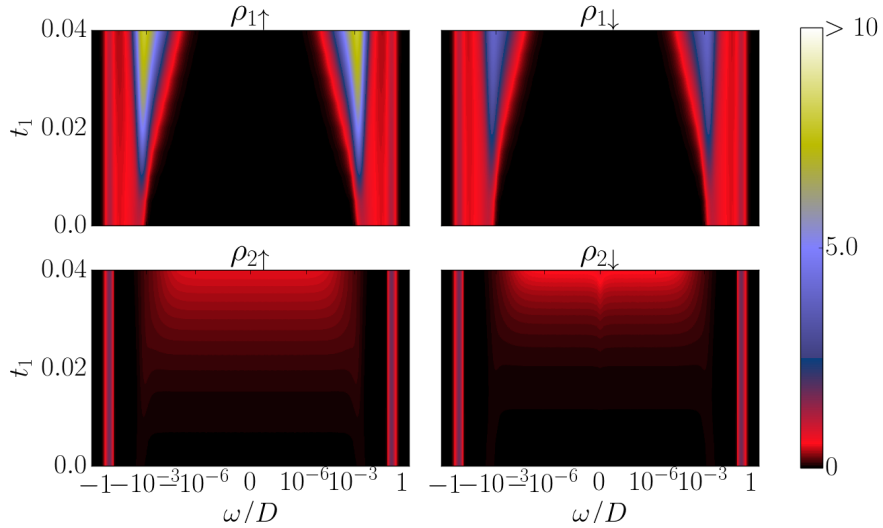


Figure 3.20: Source: By the Author

3.2. Interacting Results

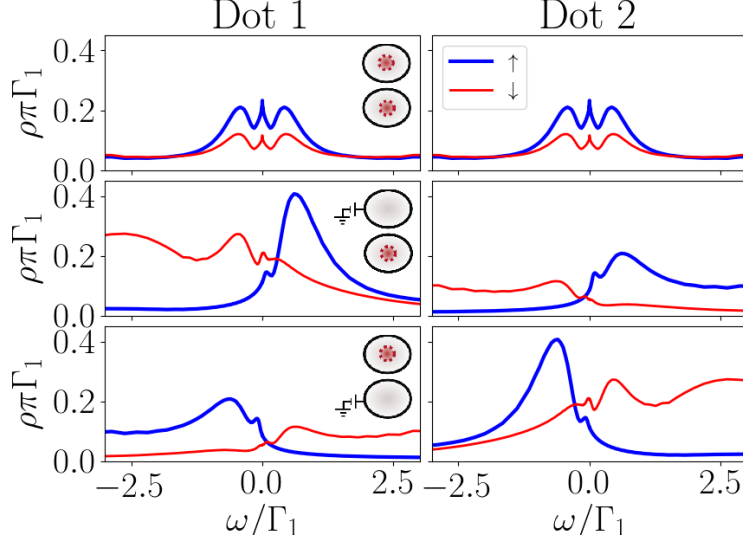


Figure 3.14: Density of states in dots 1(Left) and 2(Right) for the model ???. (a). First line (a),(b): $\epsilon_1 = \epsilon_2 = 0$. Second line (c),(d): $\epsilon_1 = 5\Gamma_1$, $\epsilon_2 = 0$. Third line (e),(f): $\epsilon_2 = -5\Gamma_1$, $\epsilon_1 = 0$. Blue bold lines: Spin- \uparrow DOS. Red thin lines: Spin- \downarrow DOS. The inset at the upper-right corner of each line indicates which dots exhibit Majorana signature, which is represented by a red dashed circle inside the dot.

3.2.2 b) Indirect Majorana after Removing Kondo with QD-interference

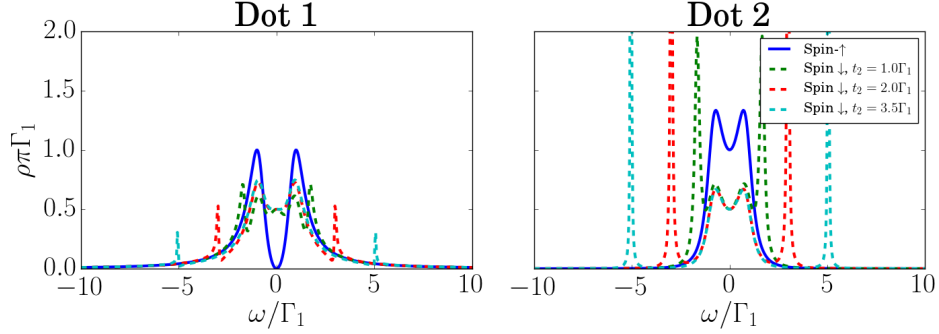


Figure 3.21: Source: *By the Author*

3.2. Interacting Results

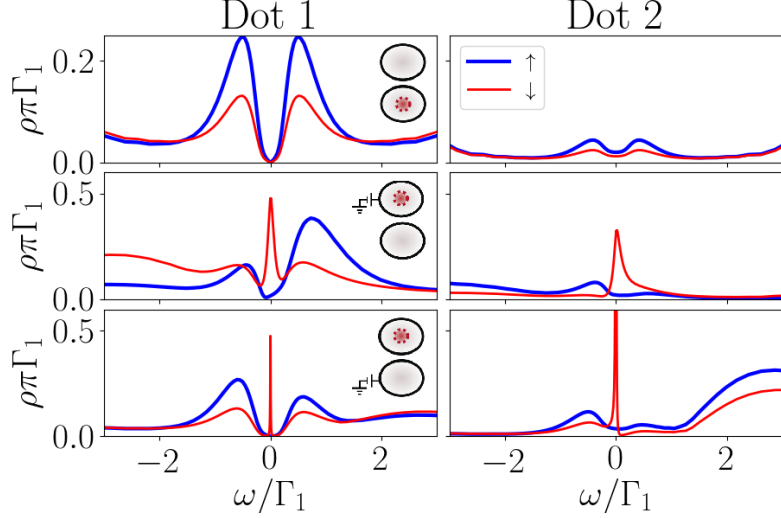


Figure 3.15: Density of states in dots 1(Left) and 2(Right) for the model ???. (b). First line (a),(b): $\epsilon_1 = \epsilon_2 = 0$. Second line (c),(d): $\epsilon_1 = 5\Gamma_1$, $\epsilon_2 = 0$. Third line (e),(f): $\epsilon_2 = -5\Gamma_1$, $\epsilon_1 = 0$. Blue bold lines: Spin- \uparrow DOS. Red thin lines: Spin- \downarrow DOS. The inset at the upper-right corner of each line indicates which dots exhibit Majorana signature, which is represented by a red dashed circle inside the dot.

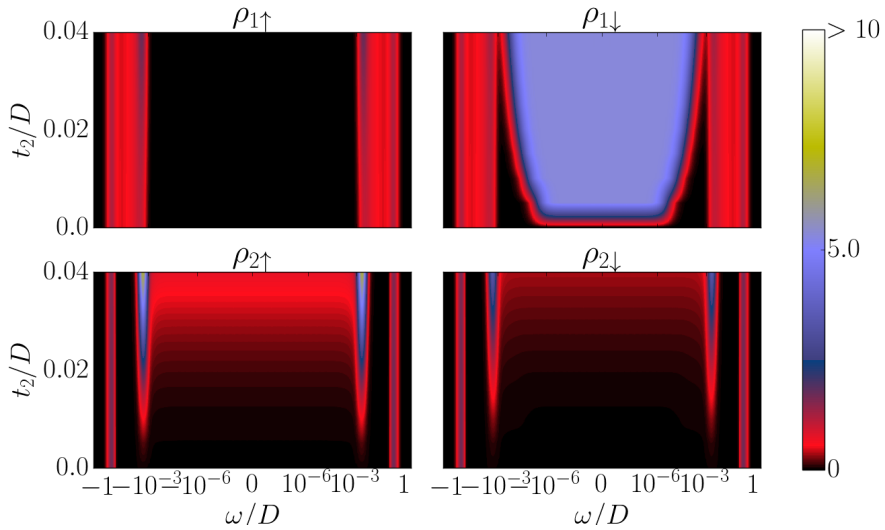


Figure 3.22: Source: By the Author

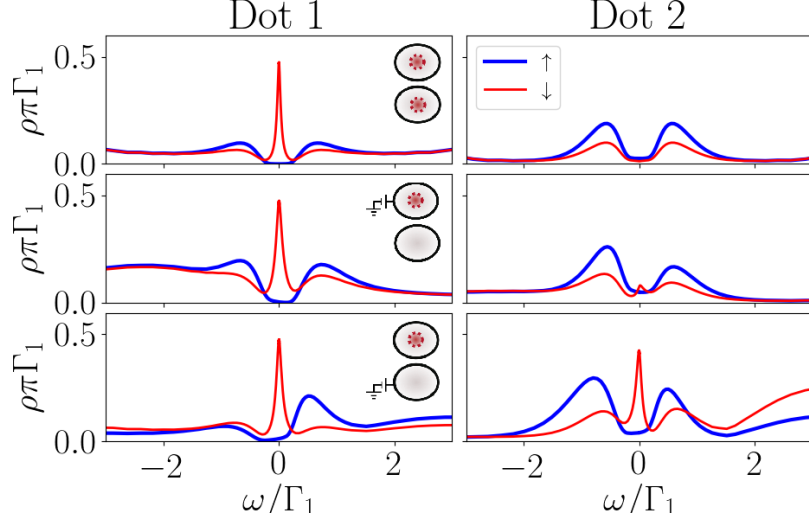


Figure 3.16: Density of states in dots 1(Left) and 2(Right) for the model ???. (c). First line (a),(b): $\epsilon_1 = \epsilon_2 = 0$. Second line (c),(d): $\epsilon_1 = 5\Gamma_1$, $\epsilon_2 = 0$. Third line (e),(f): $\epsilon_2 = -5\Gamma_1$, $\epsilon_1 = 0$. Blue bold lines: Spin- \uparrow DOS. Red thin lines: Spin- \downarrow DOS. The inset at the upper-right corner of each line indicates which dots exhibit Majorana signature, represented by a red dashed circle inside the dot.

c) Attaching the Majorana mode to the DQD (Tuning $t_1 = t_2$)

Parameters:

$$\begin{aligned} \Gamma &\sim 2.83 * 10^{-2} D, t_{dots} = 0, U_{1,2} = -2\epsilon_{1,2} = 0.5 \\ t_1 = t_2 &\in [0, 2.5 * 10^{-2} D] \end{aligned}$$

The first process consists in attaching the Majorana mode to both Quantum Dots symmetrically. For this, we scale up the coupling parameter $t_1 = t_2$ from 0 (Decoupled) to 0.02 (Completely coupled). The other parameters were chosen with an equilibrium between the dot

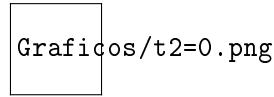


Figure 3.17: Density of states in both dots of the case where the only the first QD is attached to both Majorana and Lead (Fig.Figure 3.3 second column) . Solid lines: Spin- \uparrow DOS. Dashed lines: Spin- \downarrow DOS.

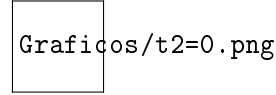


Figure 3.18: Density of states in both dots of the case where the only the first QD is attached to both Majorana and Lead (Fig. Figure 3.3 second column) . Solid lines: Spin- \uparrow DOS. Dashed lines: Spin- \downarrow DOS.

energy and Coulomb repulsion ($\varepsilon_{1,2} = -\frac{U_{1,2}}{2}$) and without inter-dot coupling $t_{dots} = 0$. These circumstances guarantee that the system preserves Particle Hole Symmetry (PHS). Thus the Density of States (DOS) of particles and holes remains equal at all instances ($\rho(-\omega) = \rho(\omega)$).

In the case where the Majorana is detached from the DQD ($t_1 = t_2 = 0$), the system favors the appearance of a three-peak at low energies as it is shown in Figure 3.24 . The central peak is produced only by the Kondo effect and the two other satellite peaks are the result of a strong correlation between both dots caused by the indirect exchange of quantum states through the Lead Appendix B.

Once the MZM the spin- \uparrow and spin- \downarrow DOS split at low energies due to the new spin- \downarrow transport channel through the Majorana mode. The spin- \downarrow DOS at the Fermi energy ($\omega = 0$) decays to the half of the spin- \uparrow DOS $\rho_\downarrow = \frac{\rho_\uparrow}{2}$. By symmetry in the dot parameters this event occurs equally for both QDs. We adopt this fact as a Majorana signature. Hence we obtain that the MZM leaks inside both quantum dots.

There is also an additional effect caused by the indirect exchange between the QDs through the Majorana mode . The consequences of this effect depend on the energy range of the Majorana couplings $t_1 = t_2$:

1. If $t_1 = t_2 \ll \Gamma$ two more satellites are formed at very low energies ($\sim t_1$) in the spin- \downarrow DOS (See Figure 3.23 Spin-down $\omega \sim 10^{-3}D$). (See Figure 3.23 Spin \uparrow , $\omega \sim 10^{-3}D$).
2. If $t_1 = t_2 \sim \Gamma$, the MZM contributes to the the growth of the spin-up satellites in the DOS. This effect produces the splitting between the spin-up and spin-down DOS. (See Figure 3.23 Spin- \downarrow , $\omega \sim 10^{-2}D$).

3.2.3 e) Transferring the MZM through gate voltage shifting ε_2 .

Parameters:

$$\Gamma \sim 2.83 * 10^{-2}D, t_{dots} = 0, U_{1,2} = -2\varepsilon_1 = 0.5, t_1 = t_2 = 0.0025$$

$$\varepsilon_2 \in [-0.25, -0.05]$$

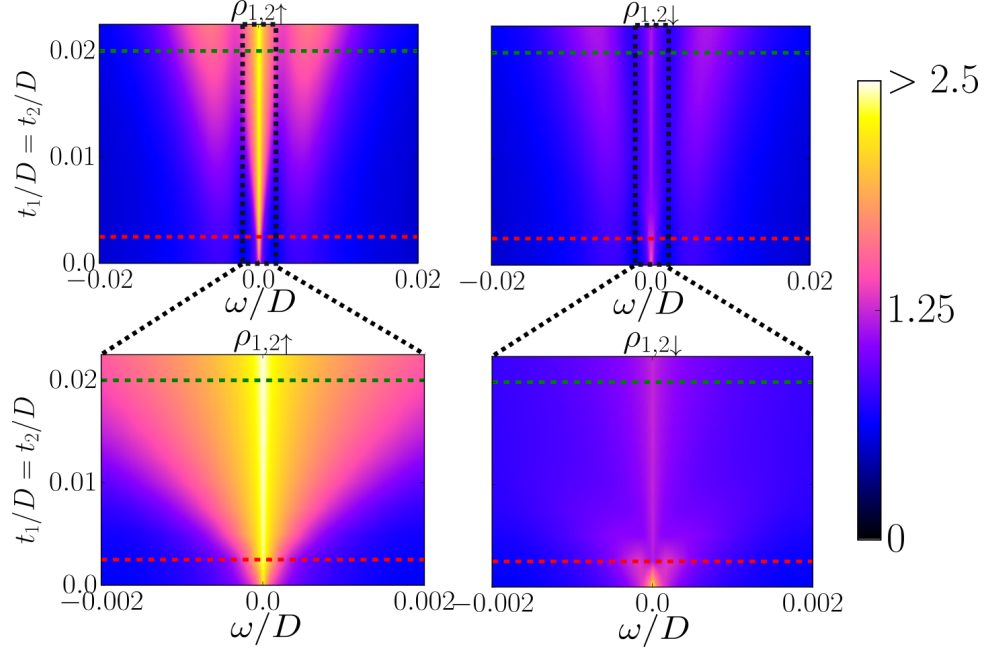


Figure 3.23: Evolution of the DOS of both QDs through $t_1 = t_2$ tuning. UP: Energy scale $\omega \sim 10^{-2}D$. DOWN: Energy scale $\omega \sim 10^{-3}D$. LEFT: Spin \uparrow . RIGHT: Spin \downarrow .

This process starts with the DQD coupled symmetrically to the Majorana mode, just as in section 3.2.2. The idea of this process is to break PHS by increasing the energy of the second QD ε_2 . This procedure should induce the Majorana to tunnel only into the first dot.

3.2. Interacting Results

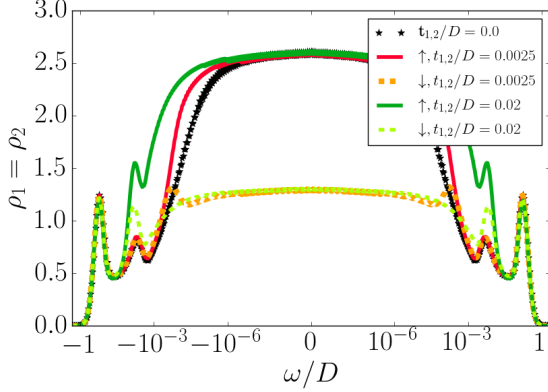


Figure 3.24: Density of states at each QD of the horizontal dashed cuts in Figure 3.23. The energy is in logarithmic scale. For $t_1 = t_2 > 0$ spin- \uparrow and spin- \downarrow DOS split near the order of $|\omega| \sim t_1, 2$. At the Fermi energy ($\omega = 0$) $\rho_\uparrow = 2\rho_\downarrow$ due to the presence of the MZM in both QDs.

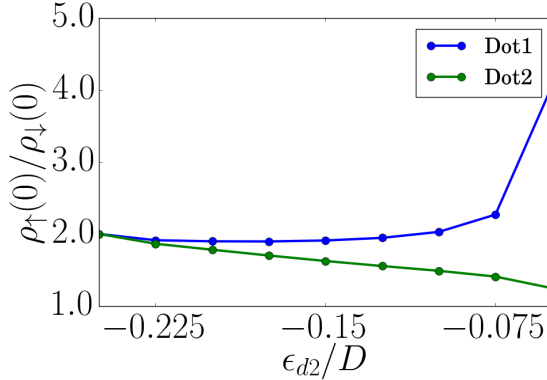


Figure 3.26: As described in section 3.2.2 the relation $\frac{\rho_\uparrow(0)}{\rho_\downarrow(0)} = 2$ constitutes a Majorana Signature . This picture evaluates shows the evolution of the relation $\frac{\rho_\uparrow(0)}{\rho_\downarrow(0)}$ for both QDs. While QD2 losses rapidly the Majorana signature, QD1 maintains it till $\varepsilon_2 \sim -0.1$.

In Figure 3.25 we observe that both, the Kondo and the MZM peaks are preserved in the first QD as well as the majorana signature (See Figure 3.26) when ε_2 is scaled up to -0.1 . However, PHS breaking will favor the growth of the spin- \uparrow hole ($w > 0$) satellite and the spin- \downarrow particle ($w < 0$) satellite.

In the second QD the DOS increases abruptly for both spins. The majorana signature is rapidly when lost . Hence, with this set-up it is actually possible to induce the Majorana to preferably tunnel QD1 in despite of QD2.

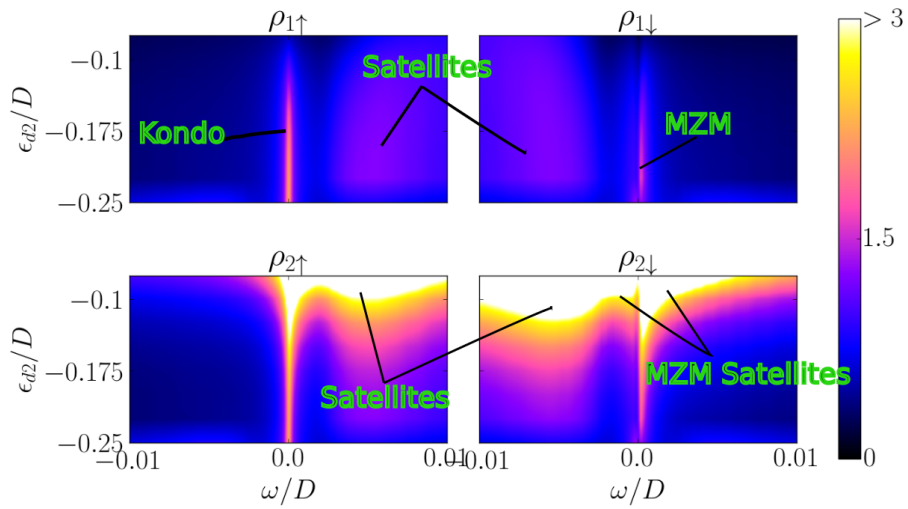


Figure 3.25: Evolution of the DOS of both QDs through the ϵ_2 tuning. UP: QD1. DOWN: QD2. LEFT: Spin \uparrow . RIGHT: Spin \downarrow .

3.3 Particle-Hole symmetric shifting of $\varepsilon_2 = \frac{U}{2}$.

 Plots/Model/Majorana-2QD-eps-converted-to.pdf

Figure 3.27: $U_1 = -2\varepsilon_{d1} = 0.5$, $\Gamma_1 = \Gamma_2$, $t_1 = t_2 = 0.02$. Variable $\varepsilon_{d2} = \frac{U_2}{2}$

 Plots/DOS/PHS-Shift_e2.png

Figure 3.28: Evolution of the QDs' DOS for the model in Figure 3.27

We start again with the symmetric model with both QDs coupled to the Majorana mode, but this time the evolution is performed over $\varepsilon_2 = \frac{U}{2}$, such that the model is always Particle-Hole symmetric. This situation is very different from the previous model (subsection 3.2.3) since the decaying of U_2 equalizes the effect of increasing the dot energy. In Figure 3.28 we observe that the DOS of QD2 increases while the QD1's DOS decreases, just as it happened in subsection 3.2.3. However, the Majorana signature remains at 2 for both dots, meaning that the Majorana is not preferably induced to tunnel to any QD despite the loss of symmetry in the dot energy.

3.4 Shifting t_2

 Plots/Model/Majorana-1QD-eps-converted-to.pdf

Figure 3.29: $U_1 = U_2 = -2\varepsilon_{d1} = -2\varepsilon_{d2} = 0.5$, $\Gamma_1 = \Gamma_2$, $t_1 = 0.02$. Variable t_2

In Figure 3.30 and Figure 3.30 we observe the evolution of DOS in the case where the second dot is smoothly connected to the Majorana, which is already attached to the first dot. The hopping parameter t_2 scales up to $0.015D$ where the model reaches the symmetry $t_2 = t_1$. The figures show that increasing t_2 leads to a drop in the DOS of QD1 while the DOS in QD2 is increased. In addition, the single peak in the first dot transforms into a three-peak due to the Majorana interference with the second dot. In ?? we also observe that the reason between the zero up-down DOS $\left(\frac{\rho_{\uparrow}(0)}{\rho_{\downarrow}(0)}\right)$ smoothly scales up to 2 in QD2. At $t_2 = 0.02$, when the is completely symmetric, the Majorana signature appears in both quantum dots. Note that the relation $\frac{\rho_{\uparrow}(0)}{\rho_{\downarrow}(0)}$ is already close to 2 at $t_2 = 0$. This implies that the second dot "feels" the Majorana even when it is not directly connected to the Majorana mode.

 Plots/2D/Shift_t2D1.png

Figure 3.30: Evolution of the DOS in the first QD

Bibliography

- [1] A. Yu Kitaev. Unpaired Majorana fermions in quantum wires. *Phys.-Usp.*, 44(10S):131, 2001. ISSN 1063-7869. doi: 10.1070/1063-7869/44/10S/S29. URL <http://stacks.iop.org/1063-7869/44/i=10S/a=S29>. 1
- [2] Jason Alicea. Majorana fermions in a tunable semiconductor device. *Phys. Rev. B*, 81(12):125318, March 2010. doi: 10.1103/PhysRevB.81.125318. URL <https://link.aps.org/doi/10.1103/PhysRevB.81.125318>. 1
- [3] Jason Alicea. New directions in the pursuit of Majorana fermions in solid state systems. *Rep. Prog. Phys.*, 75(7):076501, 2012. ISSN 0034-4885. doi: 10.1088/0034-4885/75/7/076501. URL <http://stacks.iop.org/0034-4885/75/i=7/a=076501>. 1
- [4] Dong E. Liu and Harold U. Baranger. Detecting a majorana-fermion zero mode using a quantum dot. 84(20). ISSN 1098-0121, 1550-235X. doi: 10.1103/PhysRevB.84.201308. URL <http://arxiv.org/abs/1107.4338>. 1, 3.1.2
- [5] Minchul Lee, Jong Soo Lim, and Rosa Lopez. Kondo effect in a quantum dot side-coupled to a topological superconductor. 87(24):241402. doi: 10.1103/PhysRevB.87.241402. URL <https://link.aps.org/doi/10.1103/PhysRevB.87.241402>. 1
- [6] E. Vernek, P. H. Penteado, A. C. Seridonio, and J. C. Egues. Subtle leakage of a majorana mode into a quantum dot. 89(16):165314. doi: 10.1103/PhysRevB.89.165314. URL <https://link.aps.org/doi/10.1103/PhysRevB.89.165314>. 1
- [7] M. T. Deng, S. Vaitiekėnas, E. B. Hansen, J. Danon, M. Leijnse, K. Flensberg, J. Nygård, P. Krogstrup, and C. M. Marcus. Majorana bound state in a coupled quantum-dot hybrid-nanowire system. 354(6319):1557–1562. ISSN 0036-8075, 1095-9203. doi: 10.1126/science.aaf3961. URL <http://science.sciencemag.org/content/354/6319/1557>. 1
- [8] David A. Ruiz-Tijerina, E. Vernek, Luis G. G. V. Dias da Silva, and J. C. Egues. Interaction effects on a majorana zero mode leaking into a quantum dot. 91(11):115435. doi: 10.1103/PhysRevB.91.115435. URL <https://link.aps.org/doi/10.1103/PhysRevB.91.115435>. 1, 3.2

- [9] Maissam Barkeshli and Jay D. Sau. Physical Architecture for a Universal Topological Quantum Computer based on a Network of Majorana Nanowires. *arXiv:1509.07135 [cond-mat, physics:quant-ph]*, September 2015. URL <http://arxiv.org/abs/1509.07135>. arXiv: 1509.07135. 3
- [10] Torsten Karzig, Christina Knapp, Roman M. Lutchyn, Parsa Bonderson, Matthew B. Hastings, Chetan Nayak, Jason Alicea, Karsten Flensberg, Stephan Plugge, Yuval Oreg, Charles M. Marcus, and Michael H. Freedman. Scalable designs for quasiparticle-poisoning-protected topological quantum computation with Majorana zero modes. *Physical Review B*, 95(23):235305, June 2017. doi: 10.1103/PhysRevB.95.235305. URL <https://link.aps.org/doi/10.1103/PhysRevB.95.235305>. 3
- [11] Alexander Cyril Hewson. *The Kondo Problem to Heavy Fermions*. Cambridge University Press, April 1997. ISBN 978-0-521-59947-4. Google-Books-ID: fPzgHneNFDAC.
- [12] Kenneth G. Wilson. The renormalization group: Critical phenomena and the Kondo problem. *Reviews of Modern Physics*, 47(4):773–840, October 1975. doi: 10.1103/RevModPhys.47.773. URL <https://link.aps.org/doi/10.1103/RevModPhys.47.773>.
- [13] M. A. Ruderman and C. Kittel. Indirect Exchange Coupling of Nuclear Magnetic Moments by Conduction Electrons. *Physical Review*, 96(1):99–102, October 1954. doi: 10.1103/PhysRev.96.99. URL <https://link.aps.org/doi/10.1103/PhysRev.96.99.3.2,B>
- [14] Tadao Kasuya. A Theory of Metallic Ferro- and Antiferromagnetism on Zener’s Model. *Progress of Theoretical Physics*, 16(1):45–57, July 1956. ISSN 0033-068X. doi: 10.1143/PTP.16.45. URL <https://academic.oup.com/ptp/article/16/1/45/1861363>.
- [15] Kei Yosida. Magnetic Properties of Cu-Mn Alloys. *Physical Review*, 106(5):893–898, June 1957. doi: 10.1103/PhysRev.106.893. URL <https://link.aps.org/doi/10.1103/PhysRev.106.893.3.2,B>
- [16] H. R. Krishna-murthy, J. W. Wilkins, and K. G. Wilson. Renormalization-group approach to the Anderson model of dilute magnetic alloys. 1. Static properties for the symmetric case. *Phys.Rev.*, B21:1003–1043, 1980. doi: 10.1103/PhysRevB.21.1003. A.1, A.1
- [17] Michael Sindel. *Numerical Renormalization Group studies of Quantum Impurity Models in the Strong Coupling Limit*. Text.PhDThesis, Ludwig-Maximilians-Universitat Munchen, January 2005. URL <https://edoc.ub.uni-muenchen.de/3115/>. A.1
- [18] Ralf Bulla, Theo A. Costi, and Thomas Pruschke. Numerical renormalization group method for quantum impurity systems. *Reviews of Modern Physics*, 80(2):395–450, April 2008. doi: 10.1103/RevModPhys.80.395. URL <https://link.aps.org/doi/10.1103/RevModPhys.80.395>. A.1

Appendix A

Appendix

A.1 From the logarithmic discretization to the Wilson's chain.

Logarithmic Discretization:

We start with an Anderson model Hamiltonian such as the one in (??) without magnetic field

$$H = \frac{U}{2} + \sum_{\sigma} \left[\left(\varepsilon_d + \frac{U}{2} \right) d_{\sigma}^{\dagger} d_{\sigma} + \frac{U}{2} (d_{\sigma}^{\dagger} d_{\sigma} - 1)^2 + \sum_{\mathbf{k}} \varepsilon_{\mathbf{k}} c_{\mathbf{k}\sigma}^{\dagger} c_{\mathbf{k}\sigma} + V_{\mathbf{k}} d_{\sigma}^{\dagger} c_{\mathbf{k}\sigma} + V_{\mathbf{k}}^* c_{\mathbf{k}\sigma}^{\dagger} d_{\sigma} \right]. \quad (\text{A.1})$$

At low-energies we can assume that QD couples only to s-wave states in the leads[16]. This implies that that the Fermi surface is contained in a single, isotropic conduction band extending inside some fixed cutoffs $-D$ and D . Thus, $\varepsilon_{\mathbf{k}}$ only depends on $|\mathbf{k}|$. This makes possible to transform the sum over \mathbf{k} in equation A.1 into an integral over ε between the energy cutoffs

$$\begin{aligned} H = \sum_{\sigma} & \left[\left(\varepsilon_d + \frac{U}{2} \right) d_{\sigma}^{\dagger} d_{\sigma} + \frac{U}{2} (d_{\sigma}^{\dagger} d_{\sigma} - 1)^2 + \int_{-D}^D d\varepsilon \varepsilon c_{\varepsilon\sigma}^{\dagger} c_{\varepsilon\sigma} \right. \\ & \left. + \int_{-D}^D \sqrt{\rho_{\sigma}(\varepsilon)} d\varepsilon V_{\varepsilon} d_{\sigma}^{\dagger} c_{\mathbf{k}\sigma} + V_{\varepsilon}^* c_{\varepsilon\sigma}^{\dagger} d_{\sigma} \right]. \end{aligned} \quad (\text{A.2})$$

Here $c_{\varepsilon\sigma}^{\dagger}$ creates an electron with energy ε and $\rho_{\sigma}(\varepsilon)$ is the density of states of the system per spin, which appears in the integral due to the change of variable from \mathbf{k} to $\varepsilon \propto |\mathbf{k}|^2$. Finally, we ignore the energy dependence of ρ and V_d and we replace them by their values in the Fermi energy (This approximation has no great relevance which is justified in [16]) and we renormalize the energy band doing the replacements $k = \frac{\varepsilon}{D}$ and $c_{k\sigma} := \sqrt{D} c_{\varepsilon\sigma}$ so that (A.2) becomes

$$H = D \sum_{\sigma} \left[\frac{1}{D} \left(\varepsilon_d + \frac{U}{2} \right) d_{\sigma}^{\dagger} d_{\sigma} + \frac{U}{2D} (d_{\sigma}^{\dagger} d_{\sigma} - 1)^2 + \int_{-1}^1 dk k c_{k\sigma}^{\dagger} c_{k\sigma} + \sqrt{\frac{\Gamma}{\pi D}} \int_{-1}^1 dk d_{\sigma}^{\dagger} c_{k\sigma} + c_{k\sigma}^{\dagger} d_{\sigma} \right] \quad (\text{A.3})$$

$$= H_d + D \sum_{\sigma} \left[\int_{-1}^1 dk k c_{k\sigma}^{\dagger} c_{k\sigma} + \sqrt{\frac{\Gamma}{\pi D}} \int_{-1}^1 dk d_{\sigma}^{\dagger} c_{k\sigma} + c_{k\sigma}^{\dagger} d_{\sigma} \right], \quad (\text{A.4})$$

where $\Gamma = \pi \rho V^2$ is associated to the lever-width [17, (3.5)]. At this point we have our model dependent of three unit-less constants $\frac{\varepsilon_d}{D}$, $\frac{U}{2D}$ and $\frac{\Gamma}{\pi D}$. The logarithmic discretization starts by defining an scaling parameter $\Lambda \geq 1$ in diving the energy domain $[-1, 1]$ into an array of intervals of the form $\{[\pm \Lambda^{-(n+1)}, \pm \Lambda^n]\}_{n \in \mathbb{N}}$, as we can observe in ???. Note that the width of these intervals is decreasing exponentially by

$$d_n = \Lambda^{-n} (1 - \Lambda^{-1}).$$

Then inside of these energy intervals we can define a set of orthonormal Fourier series of the form

$$\phi_{np}^{\pm}(\varepsilon) = \begin{cases} \frac{1}{\sqrt{d_n}} e^{\pm i \omega_n p \varepsilon} & \varepsilon \in [\pm \Lambda^{-(n+1)}, \pm \Lambda^n] \\ 0 & \text{a.o.c.} \end{cases} \quad (\text{A.5})$$

with $\omega_n := \frac{2\pi}{d_n}$ so that $\phi_{np}^{\pm}(\pm \Lambda^{-(n+1)}) = \phi_{np}^{\pm}(\pm \Lambda^{-n})$. Then we can decompose the creation operators c_k^{\dagger} into their interval-Fourier contributions as

$$c_k^{\dagger} = \sum_{np} \phi_{np}^{+}(k) c_{np\sigma}^{+\dagger} + \phi_{np}^{-}(k) c_{np\sigma}^{-\dagger} \quad (\text{A.6})$$

with the new creation operators defined as

$$c_{np\sigma}^{\pm\dagger} := (c_{np\sigma}^{\pm})^{\dagger} = \int_{-1}^1 d\varepsilon [\phi_{np}^{+}(\varepsilon)]^* c_{\varepsilon\sigma}^{\dagger}.$$

This decomposition (A.6) is a simple consequence of the orthonormality of the functions defined in (A.5). In addition we can readily proof that $c_{np\sigma}^{\pm\dagger}$ -operators satisfy the anti-commutation relations, so that they are rightful fermionic creation operators.

We can now use (A.6) to replace the k -dependent terms in hamiltonian (A.3). Then we obtain

$$\begin{aligned}
\int_{-1}^1 dk c_{k\sigma}^\dagger d_\sigma &= \int_{-1}^1 dk \left(\sum_{np} \phi_{np}^+(k) c_{np\sigma}^{+\dagger} + \phi_{np}^-(k) c_{np\sigma}^{-\dagger} \right) d_\sigma \\
&= \left(\sum_{np} \left(\int_{-1}^1 dk \phi_{np}^+(k) \right) c_{np\sigma}^{+\dagger} + \left(\int_{-1}^1 dk \phi_{np}^-(k) \right) c_{np\sigma}^{-\dagger} \right) d_\sigma \\
&= \left(\sum_{np} \left(\int_{\Lambda^{-(n+1)}}^{\Lambda^{-n}} dk \frac{e^{i\omega_n p k}}{\sqrt{d_n}} \right) c_{np\sigma}^{+\dagger} + \left(\int_{-\Lambda^{-n}}^{-\Lambda^{-(n+1)}} dk \frac{e^{-i\omega_n p k}}{\sqrt{d_n}} \right) c_{np\sigma}^{-\dagger} \right) d_\sigma \\
&= \left(\sum_{np} \sqrt{d_n} \delta_p c_{np\sigma}^{+\dagger} + \sqrt{d_n} \delta_p c_{np\sigma}^{-\dagger} \right) d_\sigma \\
&= \sqrt{1 - \Lambda^{-1}} \sum_n \Lambda^{-\frac{n}{2}} (c_{np\sigma}^{+\dagger} + c_{np\sigma}^{-\dagger}) d_\sigma. \tag{A.7}
\end{aligned}$$

And

$$\begin{aligned}
\int_{-1}^1 dk k c_{k\sigma}^\dagger c_{k\sigma} &= \sum_{n,n',p,p'} \sum_{s,s'=\pm} \left(\int_{-1}^1 k dk \phi_{np}^s(k) (\phi_{np}^{s'}(k))^* \right) c_{np\sigma}^{s\dagger} c_{n'p'\sigma}^{s'} \\
&= \sum_{n,n',p,p'} \sum_{s,s'=\pm} \left(\frac{\delta_{nn'} \delta_{ss'}}{d_n} \int_{\Lambda^{-(n+1)}}^{\Lambda^{-n}} k dk e^{is\omega_n k(p-p')} \right) c_{np\sigma}^{s\dagger} c_{n'p'\sigma}^s \\
&= \sum_{npp'} \sum_{s=\pm} \left(\frac{s}{2} \Lambda^{-2n} (1 - \Lambda^{-2}) \delta_{pp'} + \frac{1 - \delta_{pp'}}{is\omega_n(p-p')} [ke^{is\omega_n k(p-p')}]_{\Lambda^{-(n+1)}}^{\Lambda^{-n}} \right) \frac{c_{np\sigma}^{s\dagger} c_{n'p'\sigma}^{s'}}{d_n} \\
&= \frac{1}{2} (1 + \Lambda^{-1}) \sum_{np} \Lambda^{-n} (c_{np\sigma}^{+\dagger} c_{np\sigma}^+ - c_{np\sigma}^{-\dagger} c_{np\sigma}^-) \\
&\quad + \sum_n \sum_{p \neq p'} \frac{1 - \Lambda^{-1}}{2i\pi(p' - p)} (c_{np\sigma}^{+\dagger} c_{np'\sigma}^+ - c_{np'\sigma}^{-\dagger} c_{np\sigma}^-) e^{\frac{2i\pi(p-p')}{1-\Lambda^{-1}}}. \tag{A.8}
\end{aligned}$$

Thus, if we replace (A.7) and (A.8) into (A.3) we will obtain a logarithmic discretization of the hamiltonian. The next part will we to map this discretization to an iterative process that is worth for a numerical computations.

Mapping the Anderson model to a Chain-Hamiltonian

We are looking for a model just like the one we have in the right part of ???. This is because a Chain-Hamiltonian will give an iterative approximation of the Anderson model with an increasing (but still controllable) number of degrees of freedom. This will provide the rightful structure for a numerical diagonalization of the hamiltonian.

A.1. From the logarithmic discretization to the Wilson's chain.

To do this, observe from equations (A.7),(A.8) that the QD (d_σ) couples directly only to the operators with $p = 0$ ($c_{n0\sigma}^{\pm\dagger}$). The $p \neq 0$ terms will appear in the hamiltonian only because they are coupled to $c_{np\sigma}^{+\dagger}$ in Equation (A.8). Thus, as a first approximation we can neglect all terms in (A.8) with $p \neq 0$. This leaves only the first part of (A.8), so that we can define $c_{n\sigma}^{\pm\dagger} := c_{np\sigma}^{\pm\dagger}$. Let

$$f_{0\sigma}^\dagger = \sqrt{\frac{1-\Lambda^{-1}}{2}} \sum_n \Lambda^{-\frac{n}{2}} (c_{n\sigma}^{+\dagger} + c_{n\sigma}^{-\dagger}), \text{ so that } \sqrt{2} f_{0\sigma}^\dagger d_\sigma = \int_{-1}^1 dk c_{k\sigma}^\dagger d_\sigma. \quad (\text{A.9})$$

Note $\{f_{0\sigma}^\dagger, f_{0\sigma}\} = \frac{1-\Lambda^{-1}}{2} \sum_n 2\Lambda^{-n} = 1$. Replacing this in (A.3)we get

$$H = H_d + D \sum_\sigma \left[\sqrt{\frac{2\Gamma}{\pi D}} (d_\sigma^\dagger f_{0\sigma} + f_{0\sigma}^\dagger d_\sigma) + \frac{1}{2} (1 + \Lambda^{-1}) \sum_n \Lambda^{-n} (c_{n\sigma}^{+\dagger} c_{n\sigma}^+ - c_{n\sigma}^{-\dagger} c_{n\sigma}^-) \right].$$

f_0^\dagger will represent the first site of the chain-hamiltonian in ?? since no other term is coupled to the dot hamiltonian. We also have the coupling term $\xi_0 = \sqrt{\frac{2\Gamma}{\pi D}}$. It is possible to obtain the following f_m^\dagger -operators by supposing a solution of the form

$$f_{m\sigma}^\dagger = \sum_n a_{mn}^+ c_{n\sigma}^{+\dagger} + a_{mn}^- c_{n\sigma}^{-\dagger} = \sum_n \sum_{s=\pm} a_{mn}^s c_{n\sigma}^{s\dagger}, \quad (\text{A.10})$$

such that they satisfy the anti-commutation relations

$$\{f_{m\sigma}^\dagger, f_{m\sigma}\} = \delta_{mm'} \delta_{\sigma\sigma'}, \quad \{f_{m\sigma}^\dagger, f_{m'\sigma'}^\dagger\} = \{f_{m\sigma}^\dagger, f_{m\sigma}^\dagger\} = 0$$

and

$$\frac{1}{2} (1 + \Lambda^{-1}) \sum_n \Lambda^{-n} (c_{n\sigma}^{+\dagger} c_{n\sigma}^+ - c_{n\sigma}^{-\dagger} c_{n\sigma}^-) = \sum_{m=0}^{\infty} \Lambda^{-\frac{m}{2}} \xi_m (f_{m\sigma}^\dagger f_{m+1,\sigma} + f_{m+1,\sigma}^\dagger f_{m\sigma}). \quad (\text{A.11})$$

It is possible to find a solution for this system using the formula of the right part of equation A.11. Since the relation is only given between consecutive terms $m, m+1$ and we already have the coefficients for $m = 0$ ($a_{0n}^s = \sqrt{\frac{1-\Lambda^{-1}}{2}} \Lambda^{-\frac{n}{2}}$). Then it is possible to determine the upper coefficients in a recursive way starting from $m = 0$. Supposing we can obtain the m^{th} -coefficients (a_{mn}^s) and then finding iteratively the coefficients of $m+1$ ($a_{m+1,n}^s$) using the relation given by equation (A.11). This provides a numerical way for obtaining the $f_{m\sigma}^\dagger$ operators. In fact in our case, where we actually did important assumptions, the problem can be solved analytically obtaining that the final Hamiltonian is given by

$$H = H_d + D \sum_\sigma \left[\sqrt{\frac{2\Gamma}{\pi D}} (d_\sigma^\dagger f_{0\sigma} + f_{0\sigma}^\dagger d_\sigma) + \frac{1}{2} (1 + \Lambda^{-1}) \sum_{n=0}^{\infty} \Lambda^{-\frac{n}{2}} \xi_n (f_{n\sigma}^\dagger f_{n+1,\sigma} + f_{n+1,\sigma}^\dagger f_{n\sigma}) \right]. \quad (\text{A.12})$$

A.1. From the logarithmic discretization to the Wilson's chain.

with

$$\xi_n = \frac{1 - \Lambda^{-n-1}}{(1 - \Lambda^{-2n-1})^{\frac{1}{2}} (1 - \Lambda^{-2n-3})^{\frac{1}{2}}}.$$

The formal recursive-solution of this problem can be found in [18]. Note that equation (A.12) describes the chain hamiltonian model that we where looking for in ???. Note that in the limit when $n \rightarrow \infty$

$$\Lambda^{\frac{-n}{2}} \xi_n \rightarrow \frac{\Lambda^{\frac{-n}{2}} (1 - \Lambda^{-n})}{1 - \Lambda^{-2n}} \sim \frac{\Lambda^{\frac{-n}{2}}}{1 + \Lambda^{-n}},$$

which implies an exponential decaying of the hopping term in the chain.

Appendix B

Three peak appearance in the Double Quantum Dot model.

The DQD model is characterized by the formation of a new state that entangles the two Quantum dots through the leads. This produces an anti-ferromagnetic interaction between the QDs, commonly known as Ruderman-Kittel-Kasuya-Yosida (RKKY) interaction [13, 15]. As consequence, two satellite peaks will emerge in the Density of States.

To explain this phenomenon we will take a symmetric version of Hamiltonian (3.1) with $2e_i = U_i = U$, $t_i = t$ and $t_{dots} = 0$ for $i \in \{1, 2\}$.

$$H = \sum_{i,k,\sigma} \frac{U_i}{2} (d_{i\sigma}^\dagger d_{i\sigma} - 1)^2 + t(d_{+, \downarrow} + d_{+, \uparrow}^\dagger) \gamma_1 + \Gamma_i (d_{i\sigma}^\dagger c_{k\sigma} + c_{k\sigma}^\dagger d_{i\sigma}). \quad (\text{B.1})$$

The symmetry of the previous Hamiltonian is suitable to apply a base change of the form

$$d_{+,\sigma} = \frac{1}{\sqrt{2}}(d_{1\sigma} + d_{2\sigma}), \quad d_{-,\sigma} = \frac{1}{\sqrt{2}}(d_{1\sigma} - d_{2\sigma}).$$

These new operators satisfy the fermionic anti-commutation relations

$$\{d_{\pm,\sigma}, d_{\pm,\sigma}^\dagger\} = 1, \{d_{\pm,\sigma}, d_{\mp,\sigma}^\dagger\} = 0,$$

so that they may be considered as fermion operators. All lineal terms in (B.1) are trivially adapted to the new base. The repulsion potential

$$\sum_i \left(\sum_\sigma d_{i\sigma}^\dagger d_{i\sigma} - 1 \right)^2 = \left(\sum_\sigma d_{1\sigma}^\dagger d_{1\sigma} - 1 \right)^2 + \left(\sum_\sigma d_{2\sigma}^\dagger d_{2\sigma} - 1 \right)^2.$$

gives rise to a non-trivial interaction between the new states. To find this interaction we define the particle number operator

$$\hat{n}_{i,\sigma} := d_{i,\sigma}^\dagger d_{i,\sigma}.$$

So that

$$\hat{n}_{1,\sigma} = \frac{1}{2} \left(\hat{n}_{+,\sigma} + \hat{n}_{-,\sigma} + d_{+,\sigma}^\dagger d_{-,\sigma} + d_{-,\sigma}^\dagger d_{+,\sigma} \right) = \frac{1}{2} (\hat{N}_\sigma + \hat{E}_\sigma),$$

with $\hat{N} = \hat{n}_{+,\sigma} + \hat{n}_{-,\sigma}$ and $\hat{E}_\sigma = d_{+,\sigma}^\dagger d_{-,\sigma} + d_{-,\sigma}^\dagger d_{+,\sigma}$. Similarly

$$\hat{n}_{2,\sigma} = \frac{1}{2} (\hat{N}_\sigma - \hat{E}_\sigma).$$

Hence

$$\sum_i (\sum_\sigma d_{i\sigma}^\dagger d_{i\sigma} - 1)^2 = \left(\frac{\hat{N} + \hat{E}}{2} - 1 \right)^2 + \left(\frac{\hat{N} - \hat{E}}{2} - 1 \right)^2 = \frac{(\hat{N} - 2)^2 - \hat{E}^2}{2},$$

with $\hat{N} = \sum_\sigma \hat{N}_\sigma$, $\hat{E} = \sum_\sigma \hat{E}_\sigma$. Note that opeator \hat{N} represents the total occupation number inside both dots. If this occupation is different than 2 there is an imbalance between particles and dots that is punished by this term. The term E^2 is much more interesting since this one is the responsible for the emergence of satellite peaks in the DOS. To understand what it makes it is simple to observe its results when applied to a based ordered by $|+, -\rangle$.

$$\hat{E}^2 |\uparrow, 0\rangle = \hat{E} |0, \uparrow\rangle = |\uparrow, 0\rangle$$

$$\hat{E}^2 |\uparrow, \downarrow\rangle = \hat{E} (|0, \uparrow\downarrow\rangle + |\uparrow\downarrow, 0\rangle) = 2|\uparrow, \downarrow\rangle - 2|\downarrow, \uparrow\rangle$$

The new Hamiltonian

$$H = \sum_\sigma \frac{U}{4} \left((\hat{N} - 2)^2 - \hat{E}^2 \right) + \frac{t}{\sqrt{2}} (d_{+, \downarrow} + d_{+, \downarrow}^\dagger) \gamma_1 + \frac{\Gamma}{\sqrt{2}} \sum_k (d_{+, \sigma}^\dagger c_{k\sigma} + c_{k\sigma}^\dagger d_{+, \sigma}) \quad (\text{B.2})$$

is represented in ??

We can explain this three-peak as the result of a new strong coupling interaction characterized by the spin exchange between both dots.

In addition, the spin-up DOS at the Fermi energy grows faster than the spin-down DOS, breaking the initial spin-symmetry when $t_1 = t_2 = 0$. At $t_1 = t_2 = 0.02D$ the spin-up DOS at the fermi energy doubles the spin-down DOS which implies that the Majorana signature is present in both dots. Indeed ?? shows that the relation $\frac{\rho_{\uparrow}(0)}{\rho_{\uparrow}(0)}$ increases continuously from 1 to 2. Note that the Majorana is completely attached when the coupling t_1 reaches the order of $0.01D$.

B.1 Initial DQD-Majorana Hamiltonian.

$H_{N_\uparrow=0, P_\downarrow=-1}$:

$$\begin{aligned} |\downarrow, \downarrow, \downarrow\rangle &\rightarrow \left[\begin{array}{cccc} \varepsilon_d^+ + \frac{U^+}{2} - 2h + \varepsilon_m & 0 & -\tilde{t}_{+1} & \tilde{t}_{+2} \\ 0 & \frac{U^+}{2} + \varepsilon_m & \tilde{t}_{-2}^* & \tilde{t}_{-1}^* \\ 0, \downarrow, 0\rangle & \rightarrow \left[\begin{array}{cccc} -\tilde{t}_{+1}^* & \tilde{t}_{-2} & \varepsilon_{d_2} + \frac{U^+}{2} - h - \varepsilon_m & t \\ \tilde{t}_{+2}^* & \tilde{t}_{-1} & t^* & \varepsilon_{d_1} + \frac{U^+}{2} - h - \varepsilon_m \end{array} \right] \\ |\downarrow, 0, 0\rangle &\rightarrow \end{array} \right] \end{aligned}$$

B.1. Initial DQD-Majorana Hamiltonian.

$$H_{N_\uparrow=0, P_\downarrow=1} :$$

$$\begin{aligned} |0,0,0\rangle &\rightarrow \left[\begin{array}{ccccc} \frac{U^+}{2} - \varepsilon_m & 0 & \tilde{t}_{+1} & \tilde{t}_{+2} \\ 0 & \varepsilon_d^+ + \frac{U^+}{2} - 2h - \varepsilon_m & \tilde{t}_{-2}^* & -\tilde{t}_{-1}^* \\ \tilde{t}_{+1}^* & \tilde{t}_{-2} & \varepsilon_{d_1} + \frac{U^+}{2} - h + \varepsilon_m & t \\ \tilde{t}_{+2}^* & -\tilde{t}_{-1} & t^* & \varepsilon_{d_2} + \frac{U^+}{2} - h + \varepsilon_m \end{array} \right] \\ |\downarrow,\downarrow,0\rangle &\rightarrow \\ |\downarrow,0,\downarrow\rangle &\rightarrow \\ |0,\downarrow,\downarrow\rangle &\rightarrow \end{aligned}$$

$$H_{N_\uparrow=2, P_\downarrow=-1} :$$

$$|\uparrow\downarrow, \uparrow\downarrow, \downarrow\rangle \rightarrow \begin{bmatrix} 2\varepsilon_d^+ + \frac{3U^+}{2} + \varepsilon_m & 0 & \tilde{t}_{+1} & \tilde{t}_{+2} \\ 0 & \varepsilon_d^+ + \frac{U^+}{2} + 2h + \varepsilon_m & \tilde{t}_{-2}^* & -\tilde{t}_{-1}^* \\ \tilde{t}_{+1}^* & \tilde{t}_{-2} & f(d_1, d_2) + h - \varepsilon_m & -t \\ \tilde{t}_{+2}^* & -\tilde{t}_{-1} & -t^* & f(d_2, d_1) + h - \varepsilon_m \end{bmatrix}$$

with $f(d_i, d_j) = \varepsilon_{d_i} + \frac{U_i}{2} + 2\varepsilon_{d_j} + \frac{3U_j}{2}$.

$$H_{N_\uparrow=2, P_\downarrow=1} :$$

$$|\uparrow, \uparrow, 0\rangle \rightarrow \begin{bmatrix} \varepsilon_d^+ + \frac{U^+}{2} + 2h - \varepsilon_m & 0 & -\tilde{t}_{+1} & \tilde{t}_{+2} \\ 0 & 2\varepsilon_d^+ + \frac{3U^+}{2} - \varepsilon_m & \tilde{t}_{-2}^* & \tilde{t}_{-1}^* \\ -\tilde{t}_{+1}^* & \tilde{t}_{-2} & f(d_2, d_1) + h + \varepsilon_m & -t \\ \tilde{t}_{+2}^* & \tilde{t}_{-1} & -t^* & f(d_1, d_2) + h + \varepsilon_m \end{bmatrix}$$